Use of Modeling and Process Analytical Technologies in the Design of a Catalytic Amination Reaction: Understanding Oxygen Sensitivity at the Lab and Manufacturing Scales

ARTICLE *in* ORGANIC PROCESS RESEARCH & DEVELOPMENT · JANUARY 2014

Impact Factor: 2.53 · DOI: 10.1021/op400226m

10 AUTHORS, INCLUDING:

Jeremy M Merritt
Eli Lilly
43 PUBLICATIONS **680** CITATIONS
SEE PROFILE

Jared W. Fennell
Eli Lilly
6 PUBLICATIONS **21** CITATIONS
SEE PROFILE

Neil J. Kallman
Eli Lilly
6 PUBLICATIONS **112** CITATIONS
SEE PROFILE

Mark A. Pietz
Eli Lilly
7 PUBLICATIONS **23** CITATIONS
SEE PROFILE

Organic Process Research & Development

Article

pubs.acs.org/OPRD

Use of Modeling and Process Analytical Technologies in the Design of a Catalytic Amination Reaction: Understanding Oxygen Sensitivity at the Lab and Manufacturing Scales

Jeremy M. Merritt,*[,†] Jonas Y. Buser,[†] Alison N. Campbell,[†] Jared W. Fennell,[†] Neil J. Kallman,[†] Thomas M. Koenig,[†] Hossam Moursy,[‡] Mark A. Pietz,[†] Norma Scully,[‡] and Utpal K. Singh[†]

[†]Small Molecule Design and Development, Lilly Research Laboratories, Eli Lilly and Company, 1400 West Raymond Street, Indianapolis, Indiana 46221, United States

[‡]Manufacturing Science and Technology Business, Eli Lilly SA, Dunderrow, Kinsale, County Cork, Ireland

Supporting Information

ABSTRACT: A mechanistic approach was undertaken to understand the oxygen sensitivity of a Pd-catalyzed amination reaction used in the synthesis of an active pharmaceutical ingredient. FlowNMR and dissolved oxygen probes were used as process analytical technology alongside kinetic and unit operation models to better characterize the oxidative deactivation pathways of the catalyst. Interplay between ligand excess, oxygen inertion, and additional degassing due to reflux were all found to contribute to reaction rate variability. This mechanistic approach allowed for appreciation and clear communication of the risks, development of protocols to mitigate those risks, and successful scale-up under rapid development timelines.

INTRODUCTION

The utility of Pd-catalyzed amination reactions for forming C−N bonds is well established.[1−5] Emphasis has been on the development of ligands, whereby steric and electronic properties can be varied, to tune desired properties or steps of the catalytic cycle. Phosphine ligands are often used to activate and stabilize Pd(0) complexes, however, these catalytic systems can be sensitive to oxidation which can compromise their utility resulting in variability in reaction rate or completion. While standard glovebox or inertion techniques are routinely applied at the lab scale, the appreciation for an oxygen-sensitive system to be adequately addressed at scale up to commercial manufacture equipment can be hard to assess without a level of understanding of the catalyst system. Additional concerns related to an oxygen-sensitive system are made apparent because process optimization will often push to run chemistry with higher substrate to catalyst loadings. Reducing the amount of precious metals or proprietary ligands can offer significant materials cost savings but also possibly reduce or remove the need for downstream metal scavenging in cases where metals are retained in the product.[6,7]

A Pd-catalyzed amination coupling reaction between aryl-chloride (**1**) and amine (**2**) to afford compound **3** is the reaction of interest here (Scheme 1). Modifications to the previously reported process[8] were developed to achieve better selectivity of the desired product **3** without formation of impurity **4** (Figure 1) and also to provide a single liquid phase to minimize rate variability due to mass transfer effects in the previously biphasic system. The catalyst system employed is derived from Tris(dibenzylideneacetone) dipalladium(0) ($Pd_2(dba)_3$) and bis(2-diphenylphosphinophenyl)ether (DPE-phos) precursors.

An investigation was initiated to understand the process more fully and to design an appropriate oxygen control strategy mitigating several key risks identified from a chemical development perspective. First, this process was to be transferred from 8 L scale directly to 8000 L scale. Second, the standard plant nitrogen quality differed from that used during development. The standard manufacturing nitrogen supply was isolated from air using a pressure swing absorption process which had a specification limit of 0.5% O_2 (averages 0.1−0.3%) compared to N_2 used during development, which came from liquid nitrogen boil-off which typically contained <0.001% O_2. Although switching to higher quality N_2 was possible, and ultimately done, requesting manufacturing to switch to higher quality N_2 long-term had a significant cost trade-off thus the risks needed to be adequately understood. Lastly it was important to have reproducible reaction rates because of the risk of over-reaction which could cause material to fail specifications.

To mitigate these risks the approach taken was to fundamentally understand the catalytic deactivation due to oxygen. A parallel preparation sequence with independent degassing of the reaction and catalyst solutions before adding the catalyst to the reaction mixture was found to be most robust and is the starting point for this discussion. The preparation sequence is described graphically in Figure 2. The sequence of operations was intentional and is given by the numbering scheme in the figure. Studies on the impact of oxygen on the precatalyst solution and the main reaction are reported. Given an understanding of the role and acceptable limits for oxygen, focus was directed to developing protocols to enable similar

Special Issue: Transition Metal-Mediated Carbon-Heteroatom Coupling Reactions

Received: August 16, 2013
Published: November 28, 2013

   dx.doi.org/10.1021/op400226m | *Org. Process Res. Dev.* 2014, 18, 246−256

Scheme 1. Pd-catalyzed amination reaction

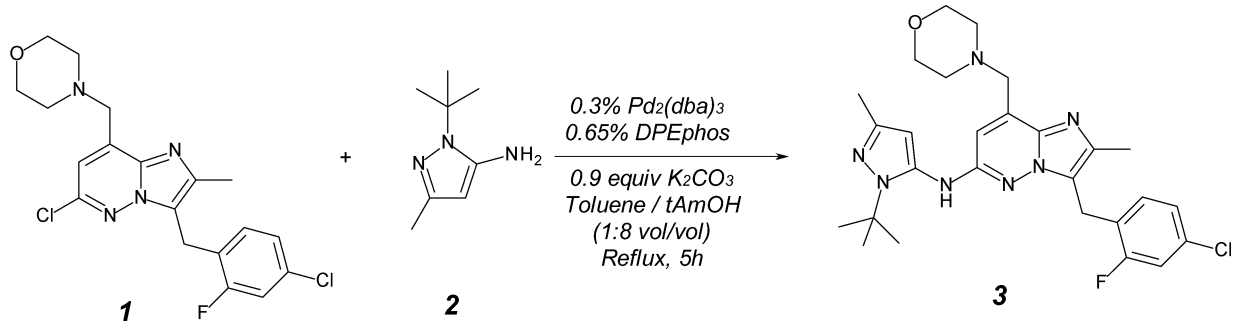

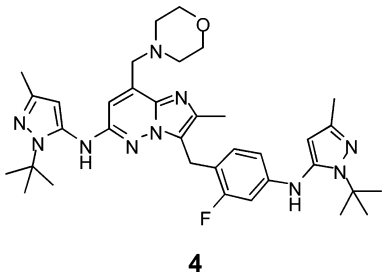

Figure 1. Impurity observed from over-reaction.

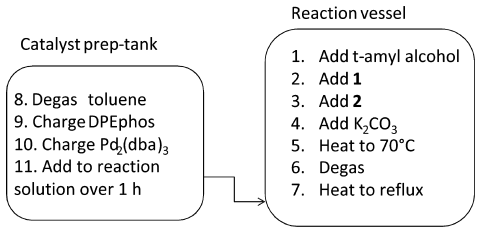

Figure 2. Graphical description of the reaction preparation. The sequence of operations was intentional and is indicated by the numbering scheme.

oxygen levels on lab and plant scales to ensure comparable performance.

RESULTS AND DISCUSSION

O_2 Sensitivity of Catalyst Preparation Solution. The first objective was to study the catalyst preparation separate from the amination reaction to understand its behavior and sensitivity to oxygen. The operating mechanism showing catalyst resting state Pd(DPEphos)(dba) (**6**) and the likely active catalyst, Pd(DPEphos) (**8**) are described in the catalytic cycle of a Pd-catalyzed amination summarized in Figure 3. The mechanism for the catalytic cycle is based on the work of Singh et al.[9] with oxidative addition of **8** to the aryl-chloride (ArCl) taking place first, followed by amine (RNH_2) coordination and reductive elimination to yield product (R-NH-Ar). The possibility for off-cycle pooling of reservoir catalysts such as $Pd(DPEphos)_2$ (**7**) is also accounted for as shown in Figure 3. The impact of reservoir catalysts on reaction kinetics has been described elsewhere[10] and is discussed in the context of O_2 sensitivity below. To support this mechanism as operational in our process, process analytical technology (PAT) tools were used to enable the investigation.

In order to enable quantitative comparison of degassing techniques and oxidation measurements, dissolved oxygen (DO) sensors were used to measure O_2 concentrations in situ.

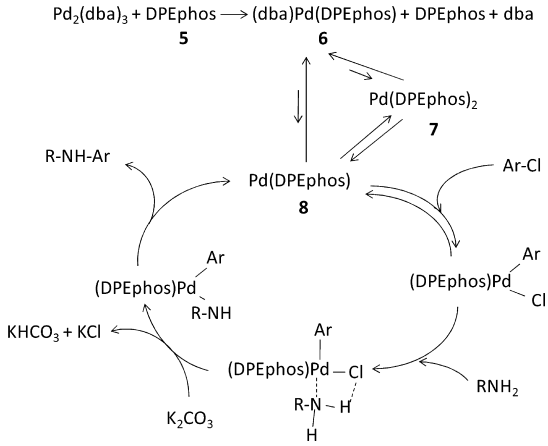

Figure 3. Assumed catalytic cycle including the resting state (**6**) and possible off-cycle reservoir species (**7**).

Probes were used in both the lab and manufacturing settings with the goal of defining reaction performance with consistent *measured* oxygen levels in the lab setting such that inertion protocols and oxygen levels could be reproduced at scale. The DO probe is calibrated before use by equilibration (saturation) of the liquid phase with air at a total pressure of 1 atm; thus, units of percent of air saturation are sometimes used to represent dissolved oxygen concentration. The equilibrium amount of dissolved oxygen is directly proportional to the headspace concentration according to Henry's Law. The gaseous % O_2 is related to % of air saturation by a dividing factor of 5 (assuming air has 20% O_2). Further details around the operation and robustness of the DO probe are found in the Experimental Section.

Headspace gas sensors are also often employed for measurement of O_2. While an in-depth comparison of the different types of measurement techniques is beyond the current scope of this work, a brief discussion is given in the Supporting Information.

^{31}P NMR (flow and tube data) was also used for reaction monitoring[11−13] to identify key species, elucidate the mechanism of oxidative catalyst deactivation, and monitor the kinetics of oxidation of the phosphine ligand under controlled O_2 environments. Details of the experimental setup of the FlowNMR system, DO probe, and O_2 control are given in the Experimental Section.

In Figure 4 are given representative ^{31}P NMR spectra collected during the time course of an oxidation experiment of just the catalyst makeup solution which was conducted using the standard concentrations of DPEphos, $Pd_2(dba)_3$, and toluene for the process (see Experimental Section). Initially,

dx.doi.org/10.1021/op400226m | Org. Process Res. Dev. 2014, 18, 246−256

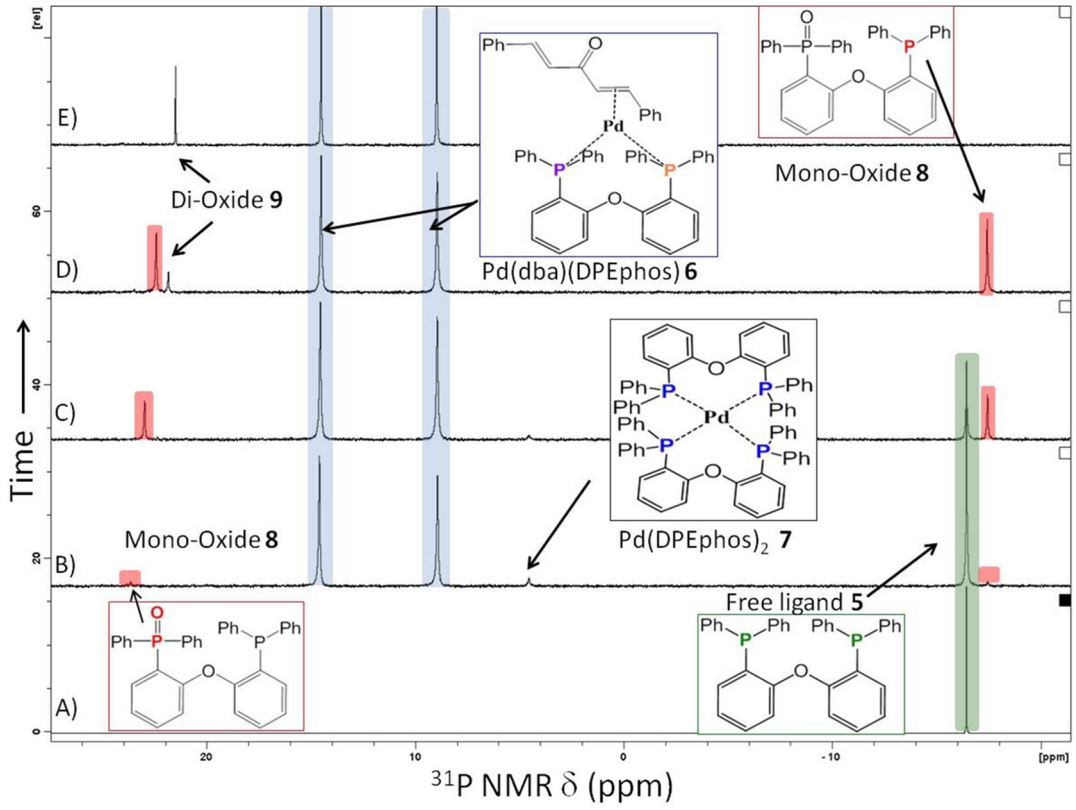

Figure 4. ^{31}P NMR spectra of time points during an experiment to examine the oxidation in the $Pd_2(dba)_3$/DPEphos catalyst makeup solution.

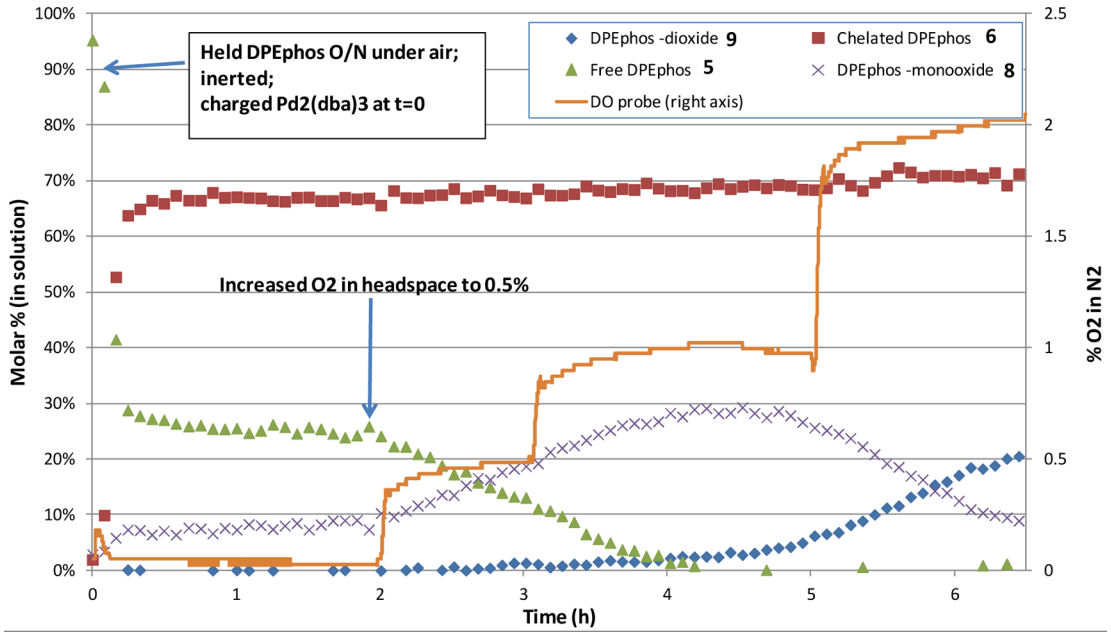

Figure 5. Time trends of ^{31}P NMR integrations illustrating the oxidation of DPEphos with $Pd_2(dba)_3$ in toluene at 20 °C. The additional trend comes from the output of the dissolved oxygen probe.

only DPEphos was charged to previously inerted toluene, and the NMR spectrum (A) contained only one peak corresponding to the two equivalent phosphorous atoms of the DPEphos (denoted as "free ligand"). Upon adding $Pd_2(dba)_3$ (B), two new resonances appeared downfield of the free ligand and were characterized by a variety of 1D and 2D hetero- and homonuclear NMR experiments to be Pd(dba)(DPEphos) (**6**). The magnetic nonequivalence of the two new resonances is attributed to differences in local phosphorous environment associated with complexed dba.[14] Upon introduction of O_2 to the system (C, D), two additional peaks are observed to grow in at the expense of the free ligand peak. These peaks are assigned to mono-oxidized DPEphos (**8**) with the upfield and downfield peaks corresponding to the unoxidized and oxidized phosphorous atoms, respectively. With additional oxygen, (E) shows the mono-oxide peaks decrease at the expense of a new

dx.doi.org/10.1021/op400226m | Org. Process Res. Dev. 2014, 18, 246−256

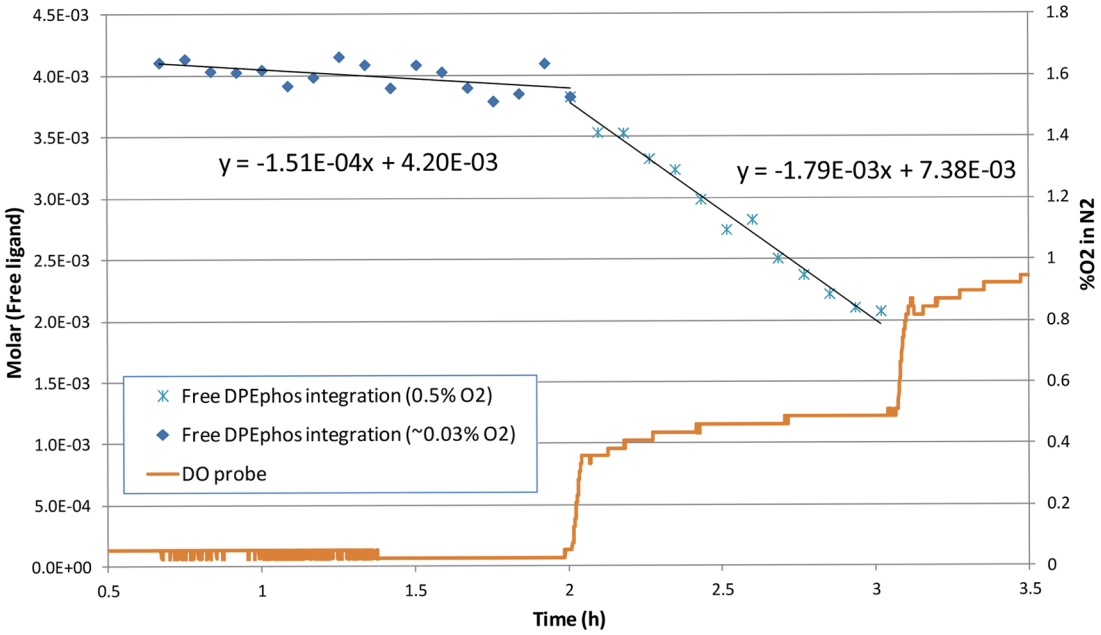

Figure 6. Time trends of the concentration of free DPEphos under oxidation conditions illustrated by the DO probe trend in toluene at room temperature with $Pd_2(dba)_3$.

peak growing in upfield of the oxidized P of **8** attributed to the dioxidized species **9**. Authentic samples of the mono- and dioxidized forms of DPEphos were synthesized, and a spiking experiment confirmed the identity of the ^{31}P NMR signals.[15] No resonances attributable to chelation of the oxidized ligand and Pd were observed.

The weak peak observed at ~5 ppm, which slightly increased in intensity when a large excess of DPEphos was added, was determined to be the bis-DPEphos Pd complex (**7**). This assignment was further confirmed by 2D ^{31}P ROESY NMR which is described in the Supporting Information. The relative ^{31}P chemical shift of the complex assigned to **7** relative to the free ligand was further supported by similar bis-species chemical shifts in the literature.[16]

With ^{31}P NMR assignments of the contributing chemical species in hand during catalyst preparation and possible oxidation products, the evolution of the concentration profiles of the species over time were followed as a function of oxygen exposure during a stress experiment. The concentration profiles are given in Figure 5.

Initially, DPEphos (**5**) was dissolved in toluene and the solution held overnight under air saturation. Solid DPEphos has been characterized as insensitive to air;[17] however, it was initially unknown to what degree this applied once dissolved. Approximately 5% oxidation to the mono-oxide (**8**) was observed after 16 h at 20 °C with full air exposure (good mixing and subsurface air sparge). Before addition of the $Pd_2(dba)_3$, the solution was degassed by flowing pure N_2 as illustrated by the DO probe trend in Figure 5. At time zero in the figure, $Pd_2(dba)_3$ was added to the ligand solution, which resulted in a small spike in the O_2 level that quickly purged back out. The ^{31}P NMR profiles showed that catalyst activation to form **6** was fast, needing <10 min to equilibrate. Although the stoichiometry of DPEphos was only in 10% excess relative to Pd, 25–30% of free DPEphos was observed after preactivation. This was the first evidence of low-potency Pd in the experiments; however, this has recently been shown to be common for $Pd_2(dba)_3$.[18] The presence of excess DPEphos due to equilibrium with the free dba was ruled out by additional ligand and dba titration.[19]

The dissolved O_2 concentration was varied systematically by introducing pseudo-step-changes in the headspace composition to allow the oxidation profile to be followed. The first step change in O_2 to 0.5% O_2 represents the specification limit of the commercial N_2 supply. On the basis of the rapid oxidation with introduction of even small amounts of O_2, the oxidation of DPEphos is clearly catalyzed by Pd, as little oxidation was observed prior to charging the Pd precursor.

Figure 6 shows the time trends for the free ligand in units of molarity. If we assume an oxidation mechanism of ligand (L) + O_2(dissolved) → mono-oxidized ligand (OL), and associated decomposition rate $-dL/dt = k[L][O_2(\text{dissolved})]$ described by the rate constant k, the pseudo-zeroth-order decay constant of $\sim 1.5 \times 10^{-4}$ mol/L h was observed under "inerted" conditions (DO probe reading ~0.03% O_2). The slope under 0.5% O_2 conditions reveals a rate constant of $\sim 1.8 \times 10^{-3}$ mol/L h. An ~10× change in the O_2 concentration appears to be directly reflected in the ~10× change in the rate constant, suggesting the decomposition is indeed first order in [O_2(dissolved)].

The zeroth-order rate constant for the "inerted" (DO reading ~0.03% O_2) conditions predicts all of the free ligand would be consumed after 27 h. Again, it should be emphasized that this scenario is for a constant flow of 0.03% O_2 purge gas and neglects the dependence on ligand concentration. If the vessel were sealed, the decomposition reaction should deplete some of the available O_2 and the stable hold time could be much longer under those conditions. A discussion on the available O_2 equivalents with respect to the ligand for a sealed system without purge is discussed below. Using the observed decay constant at 0.5% O_2 in the headspace, all of the free ligand would be consumed in ~2.2 h (again assuming zeroth-order kinetics).

While oxidation of the free ligand is occurring, there is no apparent decrease in the concentration of the chelated species **6** (Figure 5). Independent synthesis and spiking studies of the

dx.doi.org/10.1021/op400226m | Org. Process Res. Dev. 2014, 18, 246–256

oxidized ligand were performed, confirming that the oxides of DPEphos are not active (promoting or inhibiting) in the catalytic cycle of the amination reaction. No evidence for chelation of the oxidized ligands with Pd was observed in the ^{31}P NMR studies. These data support the hypothesis that the oxides do not compete with the unoxidized ligand for Pd which could promote further oxidation of the resting state of the catalyst by displacement. The data also suggest that the dissociation equilibrium constant for the Pd(dba)(DPEphos) ↔ Pd(dba) + DPEphos or 2Pd(dba)(DPEphos) + dba ↔ $Pd_2(dba)_3$ + 2DPEphos reactions (at room temperature) are shifted far towards the left; otherwise autocatalytic oxidation of the liberated free DPEphos would be expected by Pd(DPEphos) (also in equilibrium with Pd(dba)(DPEphos). At elevated temperature (as under the reaction conditions at reflux), however, one would expect the equilibrium to shift (at least somewhat) towards the dissociated complex and faster decomposition would occur. The relevance of oxidation of free-ligand on the amination reaction performance was tested and is described below.

O_2 Sensitivity of the Combined Reaction Solution. While the oxidation work described above focused on understanding the oxidation for the catalyst preparation, more understanding was needed during the amination reaction. ^{31}P NMR online monitoring of the elevated temperature reaction mixture proved difficult due to the amount of insoluble inorganic material and the fact that slight cooling in the NMR loop could result in substrate, carbonate, or KCl precipitation from the supersaturated solution formed upon cooling. Therefore, reaction aliquots were transferred into inerted NMR tubes and analyzed for reaction progress via ^{31}P NMR.

The amination reaction was typically performed at reflux (102 °C), not only to afford a faster reaction but also to mitigate much larger rate variability and stalling observed at lower temperatures. Figure 7 shows ^{31}P NMR spectra for

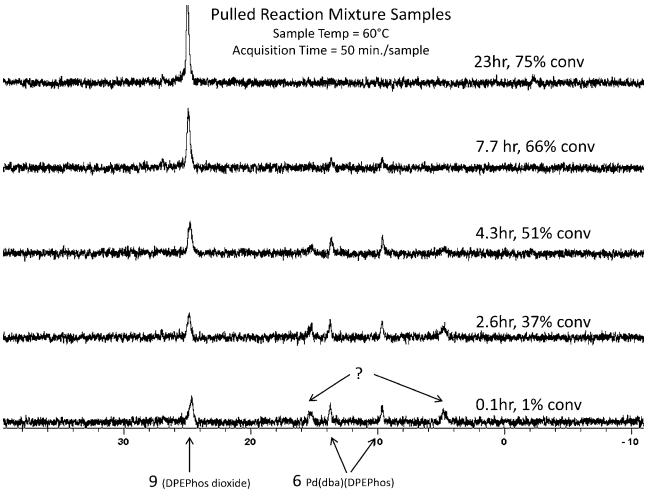

Figure 7. ^{31}P NMR for pulled reaction samples during an experiment performed at 80 °C.

samples taken during the course of a reaction at 80 °C along with HPLC reaction conversions. The reaction was observed to stall at 75% (23 h). Figure 8 shows NMR spectra during the course of a typical reaction at reflux. In this case, complete conversion was observed in 4 h. From the two data sets, we infer that the presence of the ^{31}P NMR peaks corresponding to

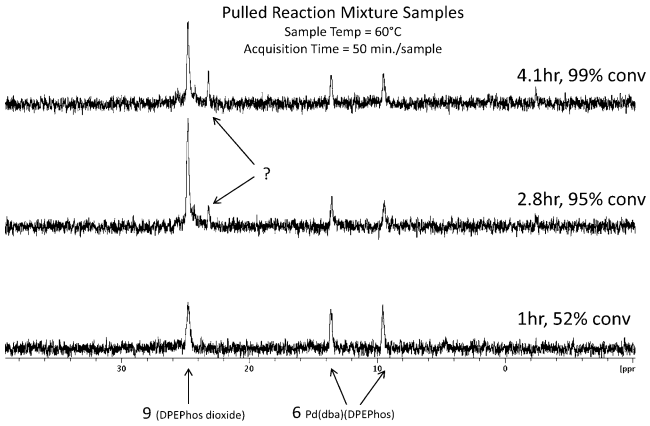

Figure 8. ^{31}P NMR for pulled reaction samples during an experiment performed at reflux (102 °C).

(Pd(dba)(DPEphos)) (**6**), the catalyst resting state, are indicative of active catalyst as these peaks are observed to disappear for the stalled reaction. Interestingly, the samples at 80 °C show two additional peaks in the NMR spectra marked with a "?" in Figure 7. At this time, they are tentatively assigned to the oxidative addition products which could build up in the tube samples due to the long acquisition times and the lower concentration of the base due to precipitation.

While the reaction at 80 °C would certainly be expected to proceed more slowly than when run at reflux (102 °C) given typical activation energies, it was initially unclear why the active catalyst was degraded and the reaction stalled at 75% conversion compared with the experiment at reflux. One hypothesis was that the act of refluxing was aiding deoxygenation, despite already sparging the system at 70 °C. To test this theory, the solvents were refluxed and then returned to 80 °C, and the reaction performed. This reaction was observed to go to completion, supporting the hypothesis that the initial sparging was not robust in terms of oxygen removal.

The data presented in Figure 7 and Figure 8 suggest that the presence of the chelated peaks in the NMR are indicative of active catalyst. On the basis of the observation that only free ligand was being oxidized and the chelated species was stable in the catalyst preparation at RT, an experiment was performed where the catalyst was preformed under inerted conditions, exposed overnight to air, and then reinerted and use-tested in a reaction monitoring catalytic activity. HPLC conversion vs time data are shown in Figure 9 for this experiment compared to those of a standard reaction. The data show the test reaction had an initial rate similar to that of the standard run but quickly started to slow. After ~5 h, the reaction had almost stalled so an additional charge of catalyst and ligand was added, resulting in complete conversion to product.

Because the initial rate of the test reaction was similar to that of a standard reaction, the initial amount of active catalyst was similar. As the test reaction progressed, the active catalyst was clearly consumed resulting in the reaction stalling. This data suggests that without the excess DPEphos to serve as sacrificial oxidant, the desired reaction rate is not maintained. Although no further oxidation of the chelated species was observed at room temperature, at reflux it is assumed that the equilibrium will be shifted further towards dissociated ligand, which may allow further oxidation of DPEphos and consequential reduction of the active catalyst.

dx.doi.org/10.1021/op400226m | Org. Process Res. Dev. 2014, 18, 246−256

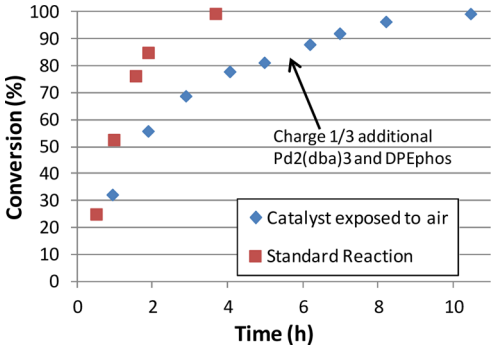

Figure 9. HPLC conversion data comparing a standard reaction with one that had the catalyst mixture exposed to air overnight and then reinerted before injection.

Klingensmith investigated the amination reaction between 4-*tert*-butylbromobenzene and morpholine, utilizing $Pd_2(dba)_3$ and Xantphos where a strong dependence of the reaction rate on Pd:ligand ratio was observed.[16] This observation was attributed to shifting the Pd(dba)(Xantphos) equilibrium toward the $Pd(Xantphos)_2$ species for higher concentrations of ligand, effectively reducing the active species concentration. This shift in concentration was experimentally observed using ^{31}P NMR. Experiments on the current system utilizing 5× DPEphos overlay quantitatively with standard conditions suggesting the analogous equilibrium is negligible as also evidenced by the lack of appreciable formation of this species in the NMR studies. This implies that excess DPEphos could be charged as a sacrificial oxidant to reduce the risk of stalling.

To further study the feasibility of using a higher O_2 content in N_2 supply at commercial scale, the risk of stalled reaction due to oxidation of the ligand was estimated by calculation of the % O_2 in N_2 that would be required to oxidize all of the ligand (assuming 1 mol O_2 consumes 2 mol of DPEphos), which is dependent on the ligand loading, liquid volume (and associated oxygen solubility), and headspace volumes for the tanks. Figure 10 illustrates the dependence of the oxygen level requirement

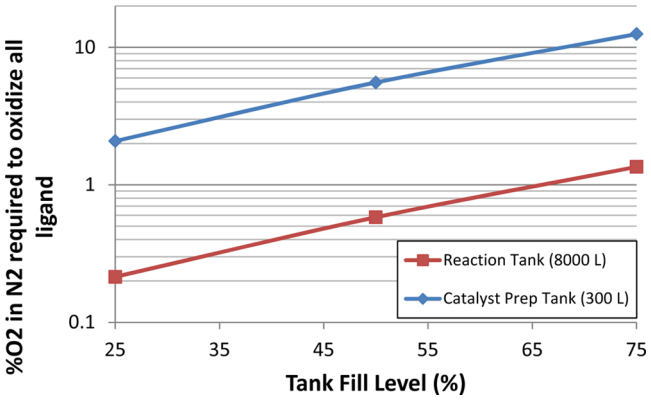

Figure 10. % O_2 in N_2 required to oxidize all of the ligand as a function of tank fill level given the current conditions.

with respect to the % fill of the tanks used for catalyst preparation and reaction assuming 0.2 mol % DPEphos and the Henry's law constants for the associated solvents. The volumes proposed in manufacturing were 25% full for the reaction tank (8000 L) and 75% full for the catalyst preparation tank (300 L). The risk assessment considering only sealed tanks that reach equilibrium in the initial degassing illustrates that, for the catalyst prep tank, using 0.5% O_2 in N_2, the risk of oxidizing all of the ligand is low. However, for the reaction tank, more than enough oxygen is present to oxidize all of the ligand. If one continued to degas a tank containing catalyst and ligand, then additional oxygen exposure would need to be considered. On the other hand, the assessment illustrates that using higher-quality N_2 reduces the risk considerably.

Scale Dependence of O_2 Removal by Reflux. It was determined by variability observed during development at small scale that reflux aids in oxygen removal even when standard lab-scale N_2 sparging was performed. In addition, there must be an associated rate of degassing as the catalyst solution was always added after the reaction mixture reached reflux. This fact makes it difficult to investigate an oxygen level failure point as the degassing rate by reflux would be expected to be scale dependent. In an idealized system at reflux, the solvent vapor pressure is equal to the atmospheric pressure (the definition of boiling); thus, the partial pressure of O_2 in the headspace is expected to tend towards zero. A real reactor with a condenser, however, is a dynamic system where the condensate could readsorb O_2 from the headspace and contain temperature gradients in the liquid and vapor phases. One hypothesis for scale dependency during reflux, therefore, is headspace turnover to exhaust the O_2 out the vent while solvent vapor is returned by the condenser. In order to estimate the scale dependence, a heat transfer calculation was performed to predict the headspace turnover due to solvent vaporization. The time-dependent O_2 partial pressure in the headspace was estimated using eq 1 which has contributions from the headspace turnover due to the volumetric flow of vapor and also return from the condensate.[20] Theoretical results are compared for a 1 L lab reactor and the 8000 L manufacturing vessels in Figure 11 utilizing experimental heat transfer and heat of vaporization data and assuming a difference in jacket and reactor temperatures of 10 °C. The model assumes initial conditions of air in the headspace the moment reflux begins, and results are plotted as % of air saturation vs time. The rate of oxygen

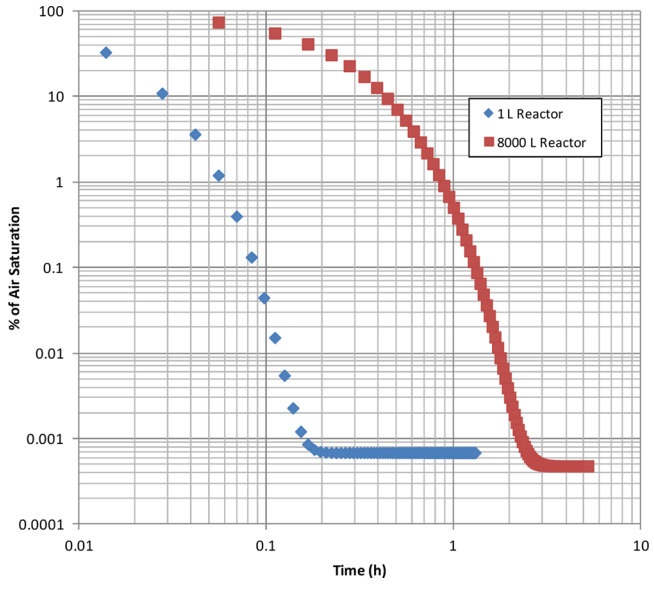

Figure 11. Oxygen degassing estimates based on heat transfer for small- and large-scale reactors.

dx.doi.org/10.1021/op400226m | *Org. Process Res. Dev.* 2014, 18, 246−256

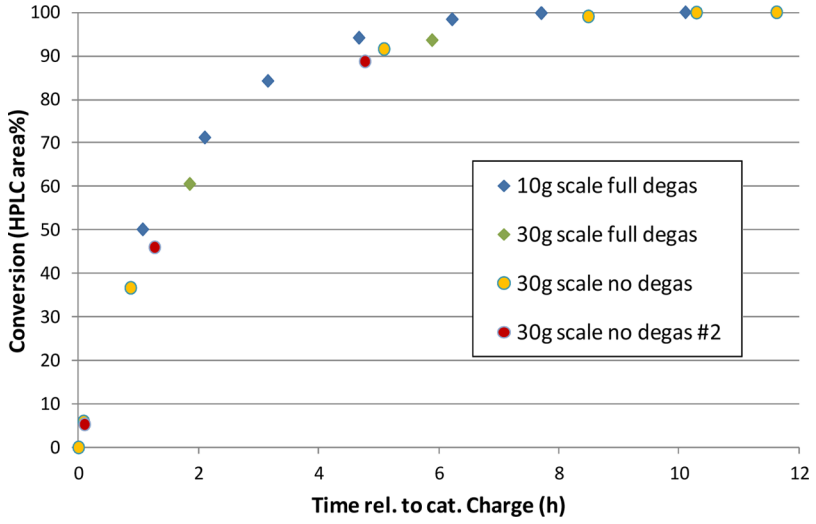

Figure 12. Reactions with and without degassing of the reaction mixture.

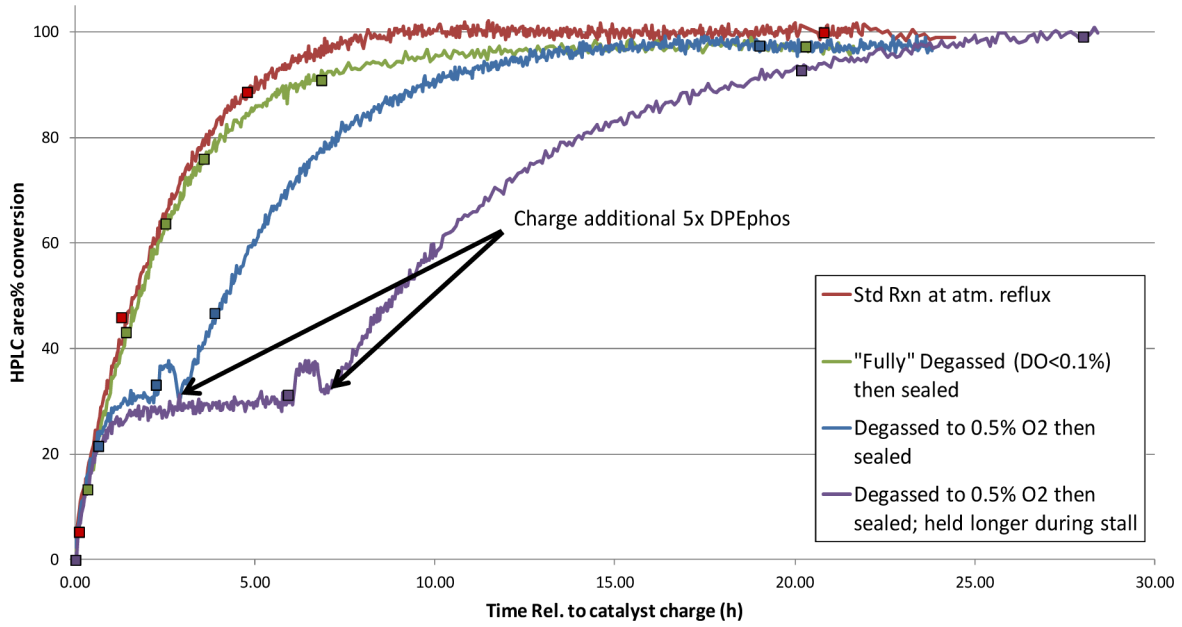

Figure 13. Conversion vs time data for reactions performed in a 1 L sealed reactor with controlled O_2 levels. Note the IR data show a baseline shift upon cooling.

return from the condensate assumes the condensate is exposed to an environment with partial pressure of 0.001 atm O_2.

$$P_{O_2}^{\text{headspace}}(t + dt) = P_{O_2}^{\text{headspace}}(t)\, e^{-\dot{V}_{\text{vapor}}^{\text{exit}} dt / V_{\text{headspace}}} + \frac{\dot{n}_{O_2}^{\text{return}} R T_{\text{vaporr}} dt}{V_{\text{headspace}}} \quad (1)$$

The model predicts that at the 1 L scale, reflux is rapid for degassing, requiring times of just a few minutes. At 8000 L scale, degassing is approximately an order of magnitude slower. To test these predictions several experiments were run with and without degassing of the reaction mixture at the 1 L scale (Figure 12). Note that the catalyst solution was always degassed. In the case of nondegassed reaction mixture, all of the catalyst solution was charged immediately upon reaching internal reflux in the condensor.

The experiments with and without degassing overlay, quantitatively illustrating that reflux can degas the system given adequate time (at this scale). Further characterization of the O_2 removal rate with time would be necessary at different scales to further develop the oxygen control strategy, especially if the initial degassing procedures prior to reflux were to be eliminated. The model results predicted that going to much larger scales or much lower temperature differential would likely be necessary to slow the degassing rate enough to enable further experimental confirmation. Note that the DO probe has an upper limit of 80 °C; thus, dissolved or headspace O_2 concentrations could not be tracked during reflux.

Due to the fact that reflux aids in degassing, it is difficult to experimentally determine the critical O_2 level that will cause a reaction to fail. Instead, to illustrate a worst case scenario several reactions were run in a 1 L sealed reactor such that they could be prepared with well-defined O_2 levels. Figure 13 shows reaction conversion data for a standard reaction at atmospheric

dx.doi.org/10.1021/op400226m | Org. Process Res. Dev. 2014, 18, 246−256

reflux, one reaction degassed to the limit of the DO probe and then sealed and heated to the normal reflux temperature, and two reactions which were degassed to contain 0.5% O_2 and then sealed and heated to the reflux temperature. The headspace to volume ratio mimicked the anticipated manufacturing conditions. In these plots concentration data predicted from an IR calibration model is shown along with the HPLC data. The reaction that was "fully" degassed to the limit of the DO probe and run sealed stalled at ~95% conversion. Stalling was attributed to slow, nonideal headspace gas mixing/diffusion during the inerting cycles, and thus higher O_2 concentrations that were held up in the head space eventually diffused to the liquid and could contribute to oxidizing the ligand. At larger scale this risk would be expected to be even larger. The two reactions which were degassed with 0.5% O_2 stalled at ~30% conversion after ~2 h. As earlier ^{31}P NMR data revealed the main pathway for catalyst deactivation is due to ligand oxidation, it was proposed that stalled reactions could be restarted by charging only additional ligand. This could have an advantage over charging both Pd and ligand as the Pd has a removal burden downstream. To test this hypothesis an additional 5× DPEphos was charged to the reactions which stalled. Before charging excess ligand, the reaction solution was cooled to 70 °C (reflected in the IR as a baseline shift) and then re-equilibrated using 0.5% O_2 to return to a state of well-defined O_2 levels. Five times the original amount of ligand was chosen as this should be enough to provide sacrificial ligand for oxidation and have enough remaining for complexation with the Pd. The IR data showed an immediate restarting of the reaction upon charging fresh ligand and heating back to reflux, and both reactions eventually reached completion.

The reaction that was held in a stalled state for a longer time period exhibited a slightly slower rate of reaction after being restarted, suggesting that some slow irreversible catalyst decomposition or aggregation to Pd black occurred during the stalled state.

Development of an Oxygen Inertion Protocol at Manufacturing Scale. Given the risks of reaction stalling and/or variability in rate and the rapid program development, the decision was made to use higher-quality N_2 for the scale-up campaign, and the feasibility of using lower-quality N_2 would be revisited in the future. Nevertheless, even neglecting N_2 quality, one must still design protocols to allow the system to reach the degassed equilibrium O_2 conditions. One additional question that was initially unknown was the oxygen level that the incoming solvents would contain.

At the lab scale, N_2 would typically be sparged subsurface for ~10 min while stirring. Utilizing the DO probe it was found that opening a fresh bottle of solvent (or using predegassed solutions) and pouring into flasks and reactors resulted in nearly 100% air saturation. Combined with experimenter differences in sparge rate and time, mixing speed and other variables, the variation in mass transfer rate (k_la) and initial O_2 level could explain some variability in the degassing quality. To develop more representative protocols for manufacturing, degassing via pressure purge cycles was implemented on a 1 L automated reactor with a 6 atm pressure capability (Mettler-Toledo RC1 with MP06 reactor), with accurate characterization of the k_la and validation of O_2 concentrations with DO probe measurements. As the gas–liquid mass transfer rate is expected to be scale dependent, better understanding of the degassing unit operation was still critical to assessing the risks for failed reactions.

The gas–liquid O_2 adsorption/desorption flux can be written as eq 2.

$$j_{O_2} = -k_l a\left(\frac{p_{O_2}}{K_H} - C_{O_2}^{liq}\right) \quad (2)$$

This is the typical diffusion-limited mass transfer equation with the solubility of O_2 replaced by the O_2 partial pressure divided by Henry's law coefficient. k_l is the associated mass transfer rate coefficient and a is the gas–liquid interfacial area. C_{O2}^{liq} is the dissolved O_2 concentration at a given time. Modeling of the dissolved O_2 concentration is thus defined by the method of inerting the headspace and assuming ideal gas and liquid mixing. In manufacturing, pressure-purge cycles would be used to inert the system; however, the model is capable of handling vacuum cycles as well as continuous sparging. Positive pressure-purge cycles were chosen to minimize possible solvent loss (as the catalyst preparation tank could not be temperature controlled and did not have a condenser) and additionally to remove concerns over air leak rates while under vacuum conditions. Pressure-purge cycles were also chosen over continuous sparging to enable higher (transient) gas velocities throughout the entire reactor to enable better mixing in the headspace to approach ideal conditions.

A mathematical model was developed in *Dynochem*[21] to predict the oxygen degassing process. The gas composition of the input flow could be adjusted in the model to compare pure N_2 vs 0.5% O_2 in N_2 for example. The output flow composition was imposed to be the headspace composition which assumes ideal mixing of the headspace. The thermodynamic removal of O_2 in each pressure purge is thus defined by the quality of N_2 input, the headspace to volume ratio, and also the change in pressure which were all adjustable parameters. The desired high-pressure limit of the purge cycles was set at 2 atm, on the basis of a safe operating range of the burst discs on the manufacturing vessels. The Henry's law constant for O_2 in toluene and *tert*-amyl alcohol was taken as the literature value for toluene (11650 Pa m^3/mol), and the temperature dependence was neglected at this stage. The key kinetic input variable is the mass transfer coefficient (k_la) for the intended operating conditions/equipment set which was treated as a fitting parameter. In general, the gas–liquid interfacial area will depend on stirring; thus, variables such as fill volume, baffling, stir rpm, impeller type, and mode of sparging will all have an impact on the desorption k_la. Temperature will also have an impact on the intrinsic rate constant (k_l), which is typically assumed to follow Arrhenius dependence.[22] The approach taken here was to measure the desorption k_la at manufacturing scale under the conditions of the solvent run. Thus, a preliminary conservative degassing protocol was delivered to aid in determination of the k_la, and this data could then be used in the model to better refine the protocol if needed. During the solvent run the pressure purging procedure was to be repeated until the oxygen level meet the limit of detection of the DO probe (~0.02% O_2) thus ensuring reproducibility of oxygen conditions at both lab and manufacturing scale.

Laboratory studies explored the differences in degassing the reaction slurry at 70 °C vs RT and showed that elevated temperature was advantageous as the k_la was faster, likely due to a pure temperature effect and the fact that the reaction mixture is a thinner slurry at this point, which should both

dx.doi.org/10.1021/op400226m | Org. Process Res. Dev. 2014, 18, 246–256

increase the degassing efficiency. In thick slurries the DO probe illustrated poor mixing resulted in inconsistent degassing.

Scale-Up to Manufacturing. The reported synthetic route was followed to synthesize **3** from **1** at the 250 kg per batch scale. Catalyst preparation and reaction were performed in 300 and 8000 L vessels respectively. Experimental DO probe data recorded for the reaction tank during the solvent run is given in Figure 14. The degassing model used a sawtooth approximation

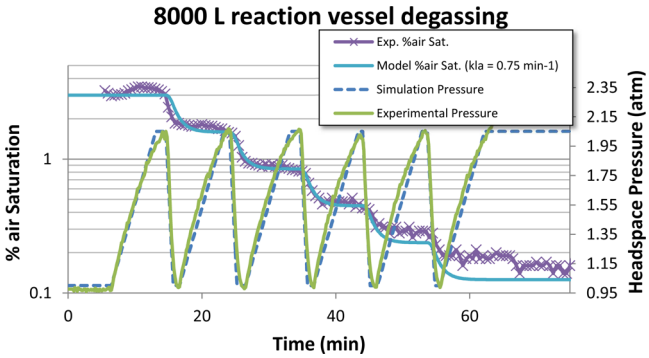

Figure 14. Experimental large-scale data from the reaction tank and model fits to extract the k_la.

of the pressure purge data. By fitting the DO data, a k_la of 0.75 min^{-1} was extracted and excellent agreement with the equilibrium O_2 levels after each purge cycle was obtained. In this case the k_la is not important in determining the overall cycle time of degassing due to the much slower rate of pressurization in the 8000 L vessel.

With the aid of the model to extract the k_la, it is possible to predict the DO levels given any pressure purge cycle scenario (assuming the same fill volumes and RPM such that mixing is not changed). Coupled with more detailed understanding of the reaction limits for oxidation of the catalyst, the model will be used to define a more refined protocol to be implemented in the future. Similar data were collected for the catalyst preparation tank.

The observation that reflux aided in degassing drove the design of the preparation sequence at scale such that the reaction contents were brought to reflux before catalyst preparation began. On average, the solutions were held at reflux for approximately 2 h before catalyst addition started. Lab-scale studies showed no detriment for prolonged heating prior to catalyst addition. Large-scale reactions were profiled by taking several HPLC samples, and an overlay of one lot with the standard lab model using the same materials is given in Figure 15.

Large scale (8000 L) data exhibited a very consistent rate of reaction across multiple batches; however, reactions at that scale were slightly slower than the lab-scale data. Incomplete reactions were not observed, and high-quality material resulted. At this time it is unclear whether the slight rate discrepancy is due to oxygen or other scale-dependent phenomenon of the chemistry and will be the subject of future investigations. Interestingly a small rate dependence is also observed comparing the 10 g (150 mL vessel) and 30 g (1 L vessel) experiments shown in Figure 12. Such scale variability highlights the need for greater understanding and the value placed in development risk assessment strategy.

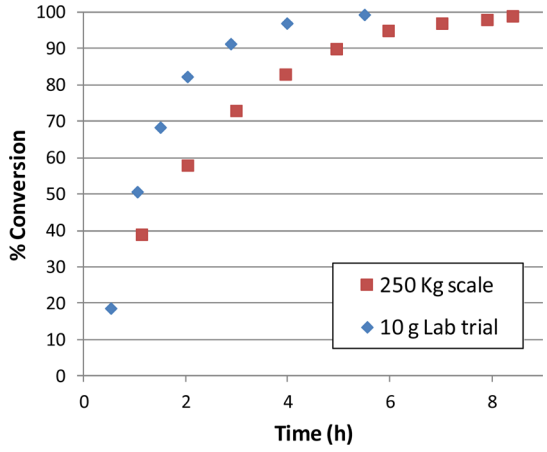

Figure 15. Comparison of kinetic data obtained at the lab and manufacturing scales.

SUMMARY

Modeling and analytical tools were used in a mechanistic approach to mitigate the scale-up risk and ensure reaction performance of a Pd-catalyzed amination reaction utilizing $Pd_2(dba)_3$ and DPEphos. The main mechanism for catalyst deactivation was elucidated to be due to ligand oxidation and the inactivity of the oxides in the catalytic cycle. Several factors were found to influence the catalytic activity including interplay of ligand excess and O_2 degassing effectiveness. No detrimental impact of reservoir catalysts such as $Pd(DPEphos)_2$ was observed which allowed demonstration of charging excess ligand as a control strategy to mitigate O_2 sensitivity or restart stalled reactions without the need of additional Pd. Reflux was found to result in additional significant degassing, however, that complicated identifying a critical O_2 limit that would cause reaction failure. Headspace turnover was proposed to explain possible scale dependency of degassing rate by reflux. Dissolved O_2 probes, used in both the lab and manufacturing setting, were extremely valuable to deliver reaction performance with consistent *measured* oxygen levels such that inertion protocols and oxygen levels could be reproduced at scale. The desire for a more mechanistic understanding drove the experimental work plan which allowed for greater understanding and clear communication of the scale-up risks.

EXPERIMENTAL SECTION

Reactions were monitored by reverse phase HPLC. HPLC conditions: XBridge C18, 4.6 mm × 75 mm, 2.5 um, 50 °C, flow 1.0 mL/min; λ = 220 nm, 3 μL injection volume; A: 20% MeCN/80% 10 mM NH_4 formate buffer, pH 4.3; B: 80% MeCN/20% 10 mM NH_4 formate buffer, pH 4.3. Gradient 15% B to 100% B in 10 min, hold at 100% B for 2 min, re-equilibrate to 15% B in 3 min. Diluent: MeOH.

N-(1-*tert*-Butyl-3-methyl-1*H*-pyrazol-5-yl)-3-(4-chloro-2-fluorobenzyl)-2-methyl-8-(morpholinomethyl)imidazo-[1,2-*b*]-pyridazin-6-amine (**3**). To a 2 L jacketed reactor, fitted with mechanical stirrer, septum, glycol-cooled condenser, and N_2 inlet was added **1** (99.90 g, 244.08 mmol, 1.00 equiv), **2** (41.20 g, 2268.88 mmol, 1.10 equiv), powder K_2CO_3 (30.40 g, 219.96 mmol, 0.90 equiv), and tAmOH (800 mL, 8 vols). The mixture was heated to 70 °C. When the mixture reached 70 °C, the mixture was sparged vigorously with N_2 via a subsurface tube for 15 min, before heating the mixture with a jacket set point of 110 °C. To a 250 mL three-necked round-bottom flask (RBF),

dx.doi.org/10.1021/op400226m | Org. Process Res. Dev. 2014, 18, 246−256

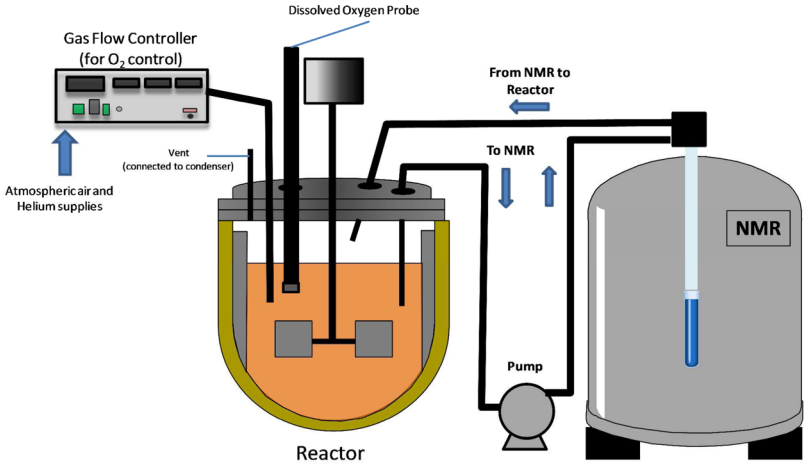

Figure 16. Illustration of the experimental setup used for the simultaneous collection of ^{31}P FlowNMR spectra with dissolved oxygen levels.

fitted with a magnetic stir bar and N_2 inlet, was added toluene (100 mL, 1 vols). The liquid was sparged vigorously with N_2 for 10 min, before DPEphos (866 mg, 1.61 mmol, 0.0066 equiv) and $Pd_2(dba)_3$ (673 mg, 734.9 μmol, 0.0030 equiv) were added. After 10 min, about half the mixture was taken up in a syringe. The catalyst was added to the reaction mixture refluxing at 102 °C via syringe pump. When the syringe was empty, the remaining catalyst mixture was taken up in the syringe. The catalyst addition was complete in 60 min. The mixture was monitored for reaction completion [% conversion = area **3**/(area **3** + **1**)*100%].

Several reactions were also trended using a Mettler-Toledo ReactIR 45m with AgX fiber ATR submersion probe (DiComp). Conversion of IR spectra to concentration units was enabled via a PLS model with corresponding HPLC data.

FlowNMR. All ^{31}P FlowNMR spectra were collected using standard Bruker ^{1}H decoupling pulse sequences with a 500 MHz Bruker Avance III spectrometer equipped with a 5 mm Bruker BBFO probe regulated to 25 °C. The reaction solutions were filtered and pumped continuously at 2.0 mL/min from the jacketed reactor to a custom NMR flowtube for spectral acquisition and back to the reactor in a completely closed loop with a Knauer Smartline 100 pump. Standard 1/16th inch PTFE tubing with 0.020 in. I.D. was used for the transfer lines. The reaction solvents used for the study were composed of fully protonated solvents with no deuterated solvent added; therefore, shims were obtained via Bruker's ^{1}H 3D and 1D TopShim procedure. The kinetic trends were extracted with MestreNova reaction monitoring software. Figure 16 shows an illustration of the experimental setup utilized for acquiring the ^{31}P FlowNMR spectra in conjunction with the dissolved oxygen probe submersed in the reactor. Quantitative control of the headspace and dissolved oxygen concentrations was achieved by subsurface sparging of gas. A calibrated gas-flow controller (MKS 4000) was used to set gas-flow rates of air and inert gas (Ar, He, N_2 used interchangeably) which were combined to generate specified O_2 levels.

Dissolved Oxygen Probe. Mettler-Ingold 6850i dissolved oxygen (DO) sensors with M400 transmitter were used to measure O_2 concentrations in situ. While dissolved oxygen probes are routinely used for aqueous solutions, few studies report on application in organic solvents. This is likely due to the material incompatibility between the gas permeable membrane (often silicone) and the solvents. The (optional) materials of construction for the membrane and probe used in this work were Kalrez and Hastelloy respectively. Good tolerance to a wide variety of solvents was found; however, membrane−solvent compatibility must still be evaluated in each case. In one instance, accelerated membrane failure (less than 1 h) was observed in the toluene-based catalyst make-up solution at >50 °C. For RT toluene studies and those in *tert*-amyl alcohol-based reaction mixtures at elevated temperatures (T < 80 °C), the membranes typically worked successfully for several weeks under continuous submersion. The digital transmitter and probe has a cutoff at 80 °C, preventing measurements above this temperature.

The DO probe measures the partial pressure of dissolved O_2, not its concentration directly. Since the probe is typically calibrated to 100% using air saturation at 1 atm, the percentage of air saturation is a common unit sometimes used. To convert partial pressure to concentration, Henry's law is employed (eq 3).

$$p_{O_2} = K_H C_{O_2}^{liq} \tag{3}$$

In principle the probe can work in any solvent system; however, a new calibration is required in each case (and at a specified temperature) due to changing membrane properties. Two gas flow controllers regulating air and argon flows were sometimes used to generate specified O_2 concentrations in the headspace and were used to qualitatively verify the probe readings.

The Henry's law constant for O_2 in toluene is K_H = 11650 Pa m^3/mol @ 298 K.[23] Thus, it can be shown that 100% air saturation results in an O_2 concentration of 64 ppm. The detection limit for the probe is estimated to be 64 ppb in toluene given the current calibration procedure and stated limit of detection of 0.1% saturation. The corresponding Henry's law data for *tert*-amyl alcohol could not be found; however, data for other alcohols suggest it is similar to toluene.[23]

■ ASSOCIATED CONTENT

Supporting Information

Discussion on gas-phase versus liquid-phase O_2 measurements, additional NMR data for assignment of bis-species (**7**), and derivation of eq 1. This material is available free of charge via the Internet at http://pubs.acs.org.

dx.doi.org/10.1021/op400226m | *Org. Process Res. Dev.* 2014, 18, 246−256

AUTHOR INFORMATION

Corresponding Author

*E-mail: merrittje@lilly.com. Telephone: (317)-651-2818.

Notes

The authors declare no competing financial interest.

REFERENCES

(1) Surry, D. S.; Buchwald, S. L. *Chem. Sci.* **2011**, *2* (1), 27−50.
(2) Hartwig, J. F. *Pure Appl. Chem.* **1999**, *71* (8), 1417−1423.
(3) Muci, A.; Buchwald, S. In *Cross-Coupling Reactions*; Miyaura, N., Ed.; Springer: Berlin Heidelberg: 2002; Vol. *219*, pp 131−209.
(4) Hartwig, J. F. *Acc. Chem. Res.* **1998**, *31* (12), 852−860.
(5) Wolfe, J. P.; Wagaw, S.; Marcoux, J.-F.; Buchwald, S. L. *Acc. Chem. Res.* **1998**, *31* (12), 805−818.
(6) Welch, C. J.; Albaneze-Walker, J.; Leonard, W. R.; Biba, M.; DaSilva, J.; Henderson, D.; Laing, B.; Mathre, D. J.; Spencer, S.; Bu, X.; Wang, T. *Org. Process Res. Dev.* **2005**, *9* (2), 198−205.
(7) Reginato, G.; Sadler, P.; Wilkes, R. D. *Org. Process Res. Dev.* **2011**, *15* (6), 1396−1405.
(8) Mitchell, D.; Cole, K. P.; Pollock, P. M.; Coppert, D. M.; Burkholder, T. P.; Clayton, J. R. *Org. Process Res. Dev.* **2011**, *16* (1), 70−81.
(9) Singh, U. K.; Strieter, E. R.; Blackmond, D. G.; Buchwald, S. L. *J. Am. Chem. Soc.* **2002**, *124* (47), 14104−14114.
(10) Ferretti, A. C.; Brennan, C.; Blackmond, D. G. *Inorg. Chim. Acta* **2011**, *369* (1), 292−295.
(11) Maiwald, M.; Fischer, H.; Kim, Y.-K.; Hasse, H. *Anal. Bioanal. Chem.* **2003**, *375* (8), 1111−1115.
(12) Gomez, M. V.; Verputten, H. H. J.; Diaz-Ortiz, A.; Moreno, A.; de la Hoz, A.; Velders, A. H. *Chem. Commun.* **2010**, *46* (25), 4514−4516.
(13) Foley, D. A.; Doecke, C. W.; Buser, J. Y.; Merritt, J. M.; Murphy, L.; Kissane, M.; Collins, S. G.; Maguire, A. R.; Kaerner, A. *J. Org. Chem.* **2011**, *76* (23), 9630−9640.
(14) A similar observation has been reported for the Pd(Xantphos)(dba) species reported in reference 16.
(15) Miyata, K.; Nakagawa, T.; Kawakami, R.; Kita, Y.; Sugimoto, K.; Nakashima, T.; Harada, T.; Kawai, T.; Hasegawa, Y. *Chem.−Eur J.* **2011**, *17* (2), 521−528.
(16) Klingensmith, L. M. *Mechanistic studies on palladium-catalyzed carbon-nitrogen bond forming reactions*; Massachusetts Institute of Technology: Cambridge, MA, 2005; Thesis: http://hdl.handle.net/1721.1/32489.
(17) STREM Chemicals Inc., Bis(2-diphenylphosphinophenyl)ether, 98% DPEphos [Material Safety Data Sheet], http://www.strem.com/catalog/v/15-0380/.
(18) Zalesskiy, S. S.; Ananikov, V. P. *Organometallics* **2012**, *31* (6), 2302−2309.
(19) The observation of ∼25% of free ligand after adding the $Pd_2(dba)_3$ was initially surprising given that the excess of ligand is only 0.1 equiv with respect to Pd in the standard lab model, which assumed 100% potency of $Pd_2(dba)_3$. Two possibilities for the discrepancy are low potency $Pd_2(dba)_3$ or an equilibrium reaction upon ligand exchange with the dba ($Pd_2(dba)_3$ + 2DPEphos ↔ 2Pd(dba)(DPEphos) + dba). To test the latter possibility, ∼30% excess $Pd_2(dba)_3$ was added to a solution containing free DPEphos, and in this instance, the DPEphos was completely consumed by the addition of additional $Pd_2(dba)_3$ to form additional **6**. As final confirmation, > 10 equiv dba was added to the solution, and no free DPEphos was observed, illustrating that the equilibrium is negligible.
(20) A derivation of eq 1 is given in the Supporting Information.
(21) *Dynochem* v.4.0.0; Scale-up Systems Inc.: Dublin, Ireland, http://scale-up.us/.
(22) Bewtra, J. K.; Nicholas, W. R.; Polkowski, L. B. *Water Res.* **1970**, *4* (1), 115−123.
(23) Battino, R.; Rettich, T. R.; Tominaga, T. *J. Phys. Chem. Ref. Data* **1983**, *12* (2), 163−178.